Editors' Suggestion

On-demand single-microwave-photon source in a superconducting circuit with wideband frequency tunability

Samarth Hawaldar,[1,2,*] Siddhi Satish Khaire,[1] Per Delsing,[3] and Baladitya Suri[1,†]

[1] *Department of Instrumentation and Applied Physics, Indian Institute of Science, Bengaluru 560012, India*
[2] *Institute of Science and Technology Austria, 3400 Klosterneuburg, Austria*
[3] *Department of Microtechnology and Nanoscience, Chalmers University of Technology, 41296 Gothenburg, Sweden*

(Received 8 September 2024; revised 4 January 2025; accepted 21 February 2025; published 18 April 2025)

In this article, we propose a method for generating single microwave photons in superconducting circuits. We theoretically show that pure single microwave photons can be generated on demand and tuned over a large frequency band by making use of Landau-Zener transitions under a rapid sweep of a control parameter. We devise a protocol that enables fast control of the frequency of the emitted photon over two octaves, without requiring extensive calibration. Additionally, we make theoretical estimates of the generation efficiency, tunability, purity, and linewidth of the photons emitted using this method for both charge- and flux-qubit-based architectures. We also provide estimates of the optimal device parameters required for these architectures to realize the device.

DOI: 10.1103/PhysRevApplied.23.044042

I. INTRODUCTION

The field of quantum information science (QIS) deals with the encoding and manipulation of information in quantum objects [1]. Communication of quantum information between spatially separated computing and/or storage nodes, i.e., between qubits, is an important component of QIS [2]. Photonic qubits are an ideal choice for this role [1,3] because of their transmission at the speed of light, weak interaction with the environment leading to robustness against external noise, and the ease of using linear optics for spatial manipulation. In this context, single-photon sources find use in quantum computation [4–6], communication [7], cryptography (primarily quantum key distribution) [8–11], and quantum sensing [12].

A practical single-photon source must be capable of on-demand generation of photons with high efficiency with frequencies tunable over a wide range [13], and it should exhibit low timing jitter in their emission [3]. Additionally, it may have the ability to generate shaped photons [2], and it should be compact so that multiple generators can be accommodated on a single chip [14]. The most commonly employed method for generating single photons in any region of the electromagnetic spectrum is to excite a two-level system (TLS), natural or artificial, and then extract a photon via spontaneous emission. In the optical regime, artificial TLSs are realized using nitrogen vacancy (NV) centers in diamond [15], single molecules [16], and quantum dots [17,18], among many other candidates. In comparison, to realize a TLS in the microwave regime, we require very low temperatures (< 100 mK) inside a dilution cryostat to avoid a thermal background of photons and to mitigate the effect of thermal excitations.

The first successful realization of a single-photon source in the microwave regime [19] made use of a transmon qubit [20] coupled to a waveguide resonator. In Ref. [19], and in the majority of the work that followed, the transmon was excited using a drive at frequency ω_{ge}, the transition frequency from the ground to the first excited state. As a consequence, a single photon is spontaneously emitted at the same frequency. Houck *et al.* [19] achieved a usable efficiency of 78%, also fulfilling the requirements of generating photons on demand and having low timing jitter due to its short excited-state lifetime ($T_1 \approx 90$ ns). Pechal *et al.* [2], using a similar architecture to that in Ref. [19], generated shaped photons with a usable efficiency of approximately 76% by making use of the second excited state of the transmon to generate a single excitation in the resonator. A further improvement to the emission bandwidth over Ref. [19] was achieved by Peng *et al.* [13] using a flux qubit directly coupled to two transmission lines, one

*Contact author: samarth.hawaldar@ist.ac.at
†Contact author: surib@iisc.ac.in

Published by the American Physical Society under the terms of the Creative Commons Attribution 4.0 International license. Further distribution of this work must maintain attribution to the author(s) and the published article's title, journal citation, and DOI.

for input and the other for output, without a resonator in the architecture. Peng *et al.* reported a usable efficiency of more than 65% over a 3-GHz range. Improvement to the generation efficiency of photons was made by Zhou *et al.* [21], who engineered the source geometry to emit photons with a peak efficiency of 87% and a tunability of greater than 1 GHz.

In the aforementioned protocols (except the work of Pechal *et al.* [2]), the excitation of the qubit is caused by drive photons at the same frequency as the single photon at the output. Therefore, the output contains drive photons alongside the desired single photons, thereby reducing the purity of the single-photon state at the output. Lu *et al.* [22] mitigated this leakage by introducing a canceling pulse at the input frequency to enhance the single-photon purity of the output. They reported a suppressed leakage of less than 0.005 photons while maintaining a usable efficiency between 71% and 99%. An alternate method for exciting the system makes use of stimulated Raman adiabatic passage (STIRAP) [23–25]. This method also enables fast preparation of a general superposition of Fock states while mitigating environmental decoherence effects and leakage by driving at a frequency distinct from that of the emitted photons. In all of these methods—even those where it is possible to tune the frequency of the emitted photon—there is the issue of needing to calibrate the drives in the system after changing the frequency of the emitter, and that of the fact that the frequency tuning is a slow process in comparison to the photon generation time.

In this work, we propose a protocol for generating high-purity single microwave photons on demand with high efficiency over a large range of frequencies using a device with a very small footprint on the chip. Hence, this protocol fulfils all the criteria of good single-photon generators, except that of the ability to shape the emitted photons. In this protocol, we use diabatic Landau-Zener transitions instead of a coherent drive tone to excite two-level systems. Within the superconducting qubit platform, we consider charge qubits and flux qubits as candidate tunable sources of single photons using this protocol. We excite either of these systems using diabatic transitions caused by a rapid sweep of a control parameter across an avoided level crossing. Since this protocol does not employ any coherent drive field, it circumvents the issue of the qubit drive tone leaking into the output and affecting the purity of the emitted single-photon state. By maximizing the diabatic transition probability while keeping the relaxation time of the qubit short, an on-demand source with an emission rate in the megahertz range can be achieved. Additionally, we propose a protocol that enables fast control of the frequency of the emitted photons *in situ* over two octaves without the need to recalibrate the system.

The remainder of this paper is structured as follows. In Sec. II, we provide a review of Landau-Zener transitions and look at their applicability to Cooper-pair boxes and flux qubits. Then, in Sec. III, we analyze a few pulse shapes and provide a pulse sequence for optimal device operation. Finally, in Sec. IV, we provide estimates of device performance for realistic parameters and present a few parameter regimes for device implementation.

II. LANDAU-ZENER TRANSITIONS FOR SINGLE PHOTON GENERATION

A. Landau-Zener transitions

The theory of Landau-Zener-Majorana-Stückelberg transitions, often simply termed Landau-Zener (LZ) transitions, describes the transition probabilities of a system in which the eigenstates (and energy eigenvalues) are tuned using an external parameter. The theory predicts that a rapid sweep of a parameter across an avoided crossing of two eigenstates (see Fig. 1) will lead to a diabatic transition from one to the other. For a TLS initially in the ground state, we start by considering a Hamiltonian with a linear time dependence. An exact solution for this Hamiltonian was shown independently by Landau [26], Zener [27], Stückelberg [28], and Majorana [29] in 1932. In general, a Hamiltonian of this form for a TLS can be written as

$$H = \hbar \begin{pmatrix} \omega_0 & D/2 \\ D/2 & \omega_0 - \beta t \end{pmatrix} \equiv \frac{\hbar \beta t}{2}\hat{\sigma}_z + \frac{\hbar D}{2}\hat{\sigma}_x \qquad (1)$$

for a time-independent β, where $\hat{\sigma}_x, \hat{\sigma}_z$ are Pauli matrices. In Eq. (1), the middle and final parts are not equal, mathematically speaking, but they are related by a gauge transformation that subtracts the same value from each diagonal term, keeping the details of the dynamics of the states the same up to a global phase. Starting in the ground state $|g\rangle$ at $t = -\infty$, solving the Schrödinger equation with the above Hamiltonian, the probability of transition to the

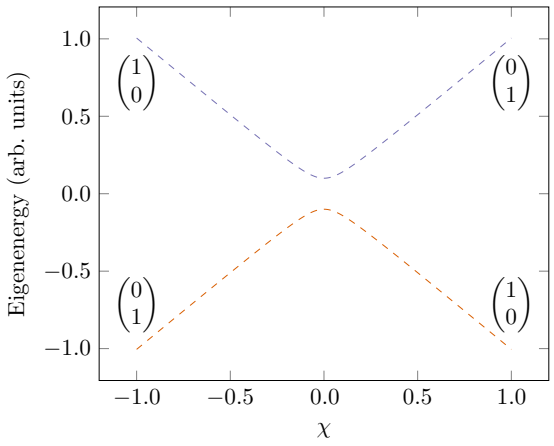

FIG. 1. Eigenvalues of the two-level LZ Hamiltonian, Eq. (1), as a function of the swept parameter $\chi = \hbar\beta t$ for $\hbar\Delta = 0.1$ The eigenstates of the Hamiltonian have been labeled at the extrema.

excited state $|e\rangle$ at $t = \infty$ is given by (see Appendix A for details)

$$P_{g\to e} = \exp\left(-\frac{\pi D^2}{2\beta}\right). \tag{2}$$

This problem can be generalized to study the evolution of an N-level system [30–33] in the presence of a linearly time-dependent tuning of the Hamiltonian of the form

$$H(t) = A + Bt, \tag{3}$$

where A and B are $N \times N$ time-independent matrices. Given the Hamiltonian described in Eq. (3), and the fact that the system is in some eigenstate $|i\rangle$ at $t = -\infty$, the generalized LZ problem aims to compute the probability of the system being in some eigenstate $|j\rangle$ at $t = \infty$. For a general N-level system, an exact solution is not yet known, but for very specific cases, solutions have been found [31–33].

B. Cooper-pair box

The Hamiltonian in Eq. (3) can, for instance, be implemented in superconducting qubit architectures such as a Cooper-pair box (CPB) or a flux qubit. A CPB is a single Josephson junction (JJ) with an associated intrinsic capacitance (C_J), connected to an external bias-voltage source V_g via a capacitance C_g [34,35] (see Fig. 2).

In the quantized charge basis $|n\rangle$, where n is the difference in the number of Cooper-pairs between the two CPB electrodes, the Hamiltonian of the CPB can be written as [34–36]

$$\hat{H} = \sum_{n\in\mathbb{Z}} \Big(E_Q (n - n_g)^2 \, |n\rangle\langle n| - \frac{E_J}{2} \left(|n\rangle\langle n+1| + |n+1\rangle\langle n|\right) \Big), \tag{4}$$

where $E_Q = 2e^2/C_\Sigma$ is the electrostatic energy of an effective capacitance C_Σ with one Cooper-pair of charge on it, E_J is the Josephson energy associated with the tunneling of Cooper pairs across the junction, and $n_g = (C_g V_g)/(2e)$ is the normalized gate charge.

Dropping the terms independent of n [37], the Hamiltonian can be rewritten in the LZ form by considering $n_g = \lambda t$ as the swept parameter, where $\lambda = C_g \dot{V}_g/(2e)$ for a constant $\dot{V}_g$. This gives

$$\hat{H} = \sum_{n\in\mathbb{Z}} \left(E_Q n^2 \, |n\rangle\langle n| - \frac{E_J}{2} \left(|n\rangle\langle n+1| + |n+1\rangle\langle n|\right) \right) - 2E_Q \lambda t \sum_{n\in\mathbb{Z}} n \, |n\rangle\langle n| = A + Bt. \tag{5}$$

When $E_Q \gg E_J$, by constraining $n_g \in [0, 1]$ [38], the system can be approximated to a TLS with a Hamiltonian given by

$$\hat{H} = \begin{pmatrix} 0 & -E_J/2 \\ -E_J/2 & E_Q - 2E_Q\lambda t \end{pmatrix} \equiv E_Q \lambda t \hat{\sigma}_z - \frac{E_J}{2}\hat{\sigma}_x, \tag{6}$$

where n_g has been redefined to be given by $n_g = \lambda t + 0.5$ such that the avoided crossing occurs at $t = 0, n_g = 0.5$. We note that more practically, as the probability of leakage due to LZ transition depends strongly on how close the system is to the avoided crossing, by constraining $n_g \in [\epsilon_g, 1 - \epsilon_g]$ for large enough ϵ_g such that the leakage outside the $n = 0, 1$ subspace can be neglected (estimates on how large ϵ_g must be can be found in Appendix E), the TLS approximation can be achieved. Comparing Eq. (6) to Eq. (1), for this system, we have $\hbar\beta = 2E_Q\lambda$. Hence, for this device, making use of Eq. (2), we obtain the probability of excitation

$$P_{\text{ex,CPB}} = \exp\left(-\frac{\pi E_J^2}{4\hbar E_Q \lambda}\right). \tag{7}$$

We can also calculate the transition frequency as a function of n_g as

$$\hbar\omega_{\text{CPB}} = \sqrt{E_J^2 + E_Q^2(1 - 2n_g)^2}. \tag{8}$$

C. Flux qubits

Another superconducting architecture in which LZ transitions can be implemented is the flux qubit. A standard flux qubit consists of three junctions in a single loop, two of which are identical with critical current I_c (and Josephson energy E_J), and the third has critical current I_c/α (and Josephson energy αE_J), where α is the junction asymmetry (see Fig. 2). The two identical junctions each have intrinsic capacitance C, and the third junction is shunted with a capacitance C_s. The Hamiltonian for this system close to the optimal point where the external flux ϕ_e can be written as $\phi_e = (n + 0.5)\Phi_0 + \delta\phi_e$ ($\Phi_0 = h/2e$ is the magnetic flux quantum, and half-integer multiples of Φ_0 are avoided crossings in the flux-qubit spectrum) can be expressed approximately in terms of a tunneling energy Δ [39–41] as

$$\hat{H} = -\gamma I_c \delta\phi_e \hat{\sigma}_z - \frac{\Delta}{2}\hat{\sigma}_x, \tag{9}$$

where $\gamma = \sqrt{1 - (1/2\alpha)^2}$.

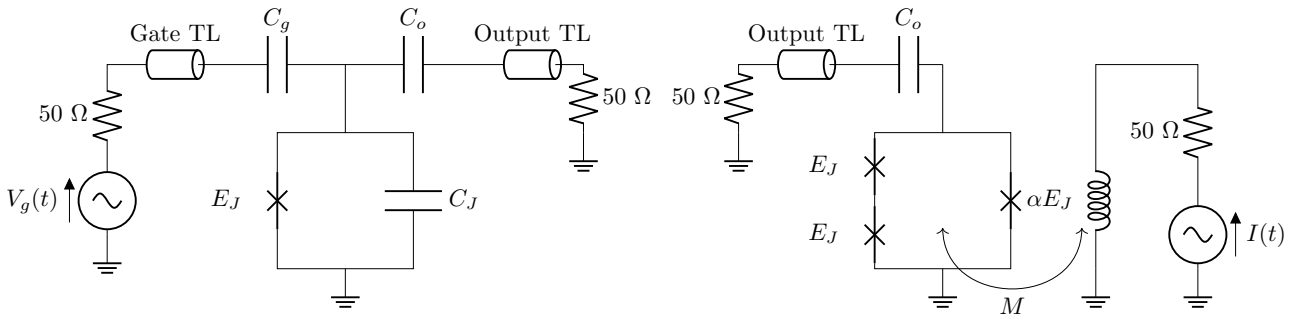

FIG. 2. Schematics for a Cooper-pair-box-based generator (left) and a flux-qubit-based generator (right).

For $\delta\phi_e = (\Phi_0/2\pi)\mu t$, we once again have an LZ-type Hamiltonian

$$\hat{H} = -\frac{\Delta}{2}\hat{\sigma}_x - \gamma E_J \mu t \hat{\sigma}_z, \tag{10}$$

with a transition frequency given by

$$\hbar\omega_{\text{flux}} = \sqrt{(2\gamma I_c \delta\phi_e)^2 + \Delta^2}. \tag{11}$$

Comparing this to Eq. (1), for this system, we once again have $\hbar\beta = 2\gamma E_J \mu$, and the probability of LZ excitation is

$$P_{\text{ex,flux}} = \exp\left(-\frac{\pi\Delta^2}{2\hbar\gamma E_J \mu}\right). \tag{12}$$

III. PROTOCOL FOR DIABATIC EXCITATIONS

As can be seen from Eqs. (2), (7), and (12), by rapidly sweeping the control parameter across an avoided crossing, a qubit can be excited (with a high probability) due to a diabatic transition. We propose to use this phenomenon to excite a superconducting qubit (charge or flux) without an input microwave excitation. The probability of excitation is closest to unity when the control parameter is swept at the greatest possible rate within the limits set by the experiment. In particular, from Eq. (2), we can see that this condition is satisfied when $\beta \gg D^2$, which translates to the conditions $\lambda \gg E_J^2/\hbar E_Q$ for the charge qubit and $\mu \gg \Delta^2/\hbar\gamma E_J$ for the flux qubit.

At the outset, if a function generator or arbitrary waveform generator (AWG) capable of providing a fixed large sweep rate (slew rate) with control over the initial and final points were available, the optimal pulsing sequence would simply involve a sweep of the control parameter χ (for a CPB, χ is $(n_g - 0.5)$, while for a flux qubit, χ is $\delta\phi_e$) from the initial value χ_i to the final (target) value χ_f at the maximum possible rate; however, most readily available AWGs define a minimum rise time (t_r) for a fixed voltage range of sweep instead of a fixed slew rate. The minimum rise time (t_r), along with the maximum output voltage of the AWG, defines the maximum slew rate possible with that instrument. This also means that a sweep range smaller than the maximum output range will result in a lower slew rate. To achieve a high slew rate, and thereby a high probability of diabatic transition, we need to execute a sweep over the full range of interest of the control parameter χ in time t_r. One way to achieve this is to add a voltage divider between the AWG and the system such that a full-range sweep on the AWG corresponds to the sweep from χ_i to χ_f at the device; however, this method requires us to work with a fixed χ_i and χ_f for the whole experiment. Another way to achieve an optimal slew rate is to use the "catapult" protocol we propose here. Using this protocol, the maximum sweep rate can be achieved independent of the values of χ_i and χ_f. This provides pulse-level control of the values of χ_i and χ_f and, in turn, enables pulse-level control of the frequency of the emitted photon.

According to this catapult protocol, we propose sweeping χ from its initial value χ_i (A in Fig. 3) to the minimum value $-\chi_0/2$ (A' in Fig. 3) in t_r, followed by a sweep from A' to the maximum value $+\chi_0/2$ (B' in Fig. 3) in t_r, and finally to the target value χ_f (B in Fig. 3) in t_r. In effect, the control parameter is first pulled back to a minimum value, and it is then rapidly catapulted over the avoided

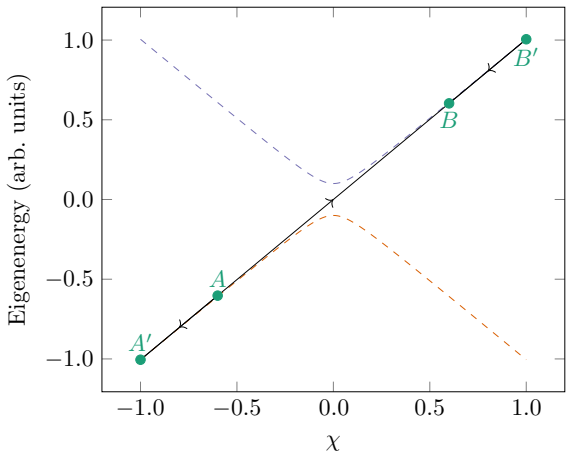

FIG. 3. Pulse sequence for changing $2\chi/\chi_0$ from -0.4 to 0.7 while performing a transition with the greatest probability afforded by the instrument.

crossing, in the minimum possible time t_r, to the maximum value. We note that the transition happens only in the second step (A'–B' in Fig. 3) of the protocol, where we traverse the avoided crossing with an associated rate of χ_0/t_r. Therefore, even though the total duration of the protocol is $3t_r$, the maximum slew rate—and in turn the transition probability—are not affected. The single photon is then spontaneously emitted at the frequency determined by the final value χ_f. Upon emission, the system returns to the ground state with the control parameter at χ_f. The catapult protocol can now be implemented in reverse to return the system to the initial control parameter χ_i while emitting another photon, this time at a frequency determined by χ_i. An important point to note here is that the protocol does not enforce any specific relationship between the initial and final points, χ_i and χ_f, respectively. This enables fast control of the emitted photon frequency in each half-cycle of the catapult protocol.

We now consider the question of the pulse shape and its effects on the transition probability. We consider four pulse shapes: linear, Gaussian, hyperbolic tangent, and exponential. Through numerical calculations, we then show that a linear sweep is sufficient for every step of the procedure (see Appendix D for details).

It is important to note that the CPB and the flux qubit have finite anharmonicity and are therefore are not pure TLSs. Therefore, we consider the effect of the rapid sweep of the control parameter on the probability of excitation of the second and higher excited states of the multilevel system. Through numerical simulations, we observe that for a given t_r, the leakage into the higher levels—which can introduce a multiphoton component in the emission—can be reduced by slightly reducing the range of the sweep A'–B' (see Fig. 3). The resultant trade-off does not severely affect the transition probability to the first excited state (see Appendix E for details).

Finally, we also consider the effect of reactive circuit elements—namely C_g for the charge qubit or the coupling inductance M for the flux qubit—on the actual pulse shape that is transmitted to the device from the control transmission line. We note that for usual experimentally feasible parameters, the time constants associated with the reactive coupling elements ($Z_0(C_g + C_o)$ for the charge qubit and M/Z_0, where $Z_0 = 50\ \Omega$ is the impedance of the environment) are in the femtosecond to picosecond range. Since the minimum rise time of currently available AWGs is in the hundreds of picoseconds to nanosecond range, we conclude that this effect can be ignored.

A. Usable efficiency

For a single-photon generator to be practically usable, the emitted photon needs to enter the output transmission line with a high probability. Hence, we define the usable efficiency η as the probability that a photon is generated and emitted into the output line:

$$\eta = P(\text{Excitation})P(\text{Emission into output}) = P_{\text{ex}}\frac{\Gamma_o}{\Gamma_{\text{tot}}}, \tag{13}$$

where Γ_o is the decay (emission) rate into the output line and Γ_{tot} $(= \Gamma_g + \Gamma_o + \Gamma_{\text{nr}})$ is the total decay rate of the TLS. For the calculation below, we assume that nonradiative decay is given by Γ_{nr}.

For a CPB, using the effective coupling capacitances to the gate and output lines $C_{g,\text{eff}}$ and $C_{o,\text{eff}}$, respectively [for the usual operating parameters, $C_{g,\text{eff}} \approx C_g$ and $C_{o,\text{eff}} \approx C_o$; see Eq. (C19) for the form of the expressions], and performing the master equation calculations for the complete Hamiltonian, we find that the photon-emission rate into the gate and output lines is $\Gamma_{g/o} \propto C^2_{g/o,\text{eff}}$ with equal proportionality constants. Hence, the usable efficiency η_{CPB} is given by

$$\eta_{\text{CPB}} = \frac{P_{\text{ex,CPB}}\Gamma_o}{\Gamma_g + \Gamma_o + \Gamma_{\text{nr}}} = \frac{\exp\left(-\dfrac{\pi E_J^2}{4\hbar E_Q \lambda}\right)}{1 + \left(C_{g,\text{eff}}/C_{o,\text{eff}}\right)^2 + \Gamma_{\text{nr}}/\Gamma_o}. \tag{14}$$

For a flux qubit, we assume that the channels of decay are to the output line and to the flux line. Assuming the capacitive coupling to the output line C_o and the mutual inductance with the flux line M, the decay rates are given by $\Gamma_o \propto \Delta C_o^2 E_J^2$ [13] and $\Gamma_f \propto M^2 E_J^2 \Delta^2/\omega_{\text{flux}}$ [20,41], respectively, with different proportionality constants, say K_o and K_f. Hence, the usable efficiency η_{flux} is

$$\begin{aligned}\eta_{\text{flux}} &= \frac{P_{\text{ex,flux}}}{1 + \Gamma_f/\Gamma_o + \Gamma_{\text{nr}}/\Gamma_0} \\ &= \frac{\exp\left(-\dfrac{\pi\Delta^2}{2\hbar E_J \mu\sqrt{1-\left(\dfrac{1}{2\alpha}\right)^2}}\right)}{1 + \dfrac{K_f M^2 \Delta}{K_o C_o^2 \omega_{\text{flux}}} + \dfrac{\Gamma_{\text{nr}}}{K_o \Delta C_o^2 E_J^2}}.\end{aligned} \tag{15}$$

For usual experimental values of $M = 0.015\ \Phi_0/\text{mA}$ [20], in the regime of high emission probability, $\Gamma_f \sim 10^3\ \text{s}^{-1}$ for $\Delta/h = 4$ GHz (and $\Gamma_f \sim 10^2\ \text{s}^{-1}$ for $\Delta/h = 1$ GHz) at $\omega_{\text{flux}} = 2\pi \times 4$ GHz, which is much lower than the $\Gamma_o \sim 10^7\ \text{s}^{-1}$ that would be designed for a high-repetition-rate device. Hence, we neglect this effect in further calculations, and for a flux qubit, we consider

$$\eta_{\text{flux}} = P_{\text{ex,flux}} \frac{\Gamma_o}{\Gamma_o + \Gamma_{\text{nr}}}. \tag{16}$$

IV. ESTIMATES, RECOMMENDED PARAMETERS, AND NOISE EFFECTS

To observe quantum effects in our devices near the region of the minimum operating energy gap, we need to ensure that the minimum excitation energy is much greater than $k_B T$ which, for a temperature of 20 mK, corresponds to a frequency $k_B T/h$ of about 400 MHz. This implies that for a thermal population of about 0.001 at 20 mK, our minimum excitation energy should be approximately 3 GHz. This does not limit our system, as the operating frequency of interest is in the range 3–12 GHz. We also consider the repetition time of the catapulting protocol (for $t_r \ll T_1$) to be $nT_1 = n/\Gamma_{\text{tot}} \approx n/\Gamma_1$ for $n \sim 5$. Here, T_1 is the excited-state lifetime of the TLS. If we consider a typical value for the lifetime $T_1 < 200$ ns, we can generate single microwave photons at a rate of around 10^6 s^{-1}.

Here, we estimate the optimal parameters for the aforementioned CPB and flux-qubit architectures by maximizing the emission probability (η) and repetition rate, while minimizing the linewidth of the emitted photon ($2\pi \times \text{FWHM} = \Delta\omega = 2\Gamma_2 = \Gamma_1 + 2\Gamma_\varphi = 1/T_1 + 2/T_\phi$). All the figures in this section are shown for an emission frequency of 6 GHz, as this lies in the center of the band of interest. In doing these calculations, we assume that the diabatic transition pulse is fast enough that decay during the pulse can be neglected. As we expect $T_1 \sim 10$ ns while $t_r \sim 300$ ps, we estimate that the probability of decay of the qubit during the catapult protocol will be less than 5%, as follows. The total duration of the LZ protocol is $3t_r$, and the desired photon frequency is determined by the final value χ_f of the control parameter; however, there is a period of time ($<1.5t_r$) during which the control parameter is not χ_f, and if the qubit were to decay during this interval ($\chi \neq \chi_f$), this would result in the emission of a photon at an undesired frequency. This probability has an upper bound given by $1 - \exp(-1.5t_r/T_1)$, which is approximately 5% for $T_1 \sim 10$ ns and $t_r \sim 300$ ps. During these calculations, we also neglect any possible non-Markovian dissipation effects that the time-dependent coupling to the environment may introduce during the LZ protocol. We also note that since the leakage probability to the levels outside the subspace of $|g\rangle$ and $|e\rangle$ is low (approximately 10^{-4}; see Appendix E), the probability of multiphoton emission is also low.

Beginning with the CPB, the system-parameter-dependent decay [42] and decoherence rates [20] are given by

$$\Gamma_{1,g/o} = \frac{RC_{g/o}^2 \omega^2}{4C_\Sigma}, \tag{17}$$

$$\Gamma_\phi = \sqrt{n_{\text{rms}}^2 \left(\frac{\partial\omega}{\partial n_g}\right)^2 + \frac{3n_{\text{rms}}^4}{4}\left(\frac{\partial^2\omega}{\partial n_g^2}\right)^2} \approx \frac{n_{\text{rms}} E_Q}{\hbar} = \frac{n_{\text{rms}}(2e^2)}{\hbar C_\Sigma}, \tag{18}$$

$$C_\Sigma \approx C_g + C_o + C_J, \tag{19}$$

where n_{rms} is the root-mean-square charge noise. For transmon systems, this is usually approximately 0.5×10^{-3} [43]. For our system, considering that the charge noise is observed to decrease with decreasing island size [44], it would be smaller. In addition to this, we can consider the effect of the voltage jitter of the AWG used, which corresponds to $V_{\text{rms}} \sim 10^{-4}$ V $\equiv n_{\text{rms}} \sim 0.5 \times 10^{-3}$ (approximately equivalent to a noise of 2 nV/$\sqrt{\text{Hz}}$ for a bandwidth of 3 GHz, as required for a 300-ps rise time). We would like to point out that V_{rms} is mostly limited by the requirement of a large bandwidth for fast pulses and can be decreased considerably if slower pulses are acceptable, such as in the case of small splittings at the avoided crossing.

We also observe from Eqs. (17) and (18) for Γ_1 and Γ_ϕ that we have a minimum possible linewidth Γ_2 if we tune C_o, since Γ_ϕ decreases with C_o while Γ_1 increases. For the optimizations presented later in this section, we take the value of Γ_2 to be close to the minimum value achievable by adjusting C_o, effectively allowing us to maintain low linewidths.

As we aim to maintain a system that can be (easily) fabricated, and we want to keep E_Q as large as possible and E_J as small as possible (this can be achieved by using a SQUID instead of a single JJ to tune the value of E_J using an external magnetic field), we fix $\Gamma_{\text{nr}} = 1$ μs^{-1} (corresponding to $T_{1,i} = 1$ μs), $C_g = 10$ aF, $C_J = 1$ fF, and $E_J/h = 1$ GHz. Additionally, we would like to tune the value of C_o to obtain the maximum usable emission probability for different sweep rates for two different levels of charge noise, $n_{\text{rms}} = 0.5 \times 10^{-3}$ and $n_{\text{rms}} = 0.05 \times 10^{-3}$. As we would also like to maintain a repetition rate ≥ 1 MHz, we would like $T_1 \leq 200$ ns. The optimized probabilities and corresponding T_1 values for different charge-noise levels are shown for this system in Fig. 4.

We observe that for a rise time of 300 ps—a value that is achievable in several commercial AWGs—for a charge noise of 0.5×10^{-3}, we have a usable efficiency of 90.6% with an optimal $C_o \approx 2.3$ fF, all while maintaining a T_1 of 33.8 ns, corresponding to a repetition rate of about 5.9 MHz (the numbers are almost the same for the lower charge noise, but the linewidths are different for the emitted photon).

Next, we analyze the prospect of using flux qubits for single-photon generation using our protocol. As a flux qubit's primary decoherence channel is due to flux noise,

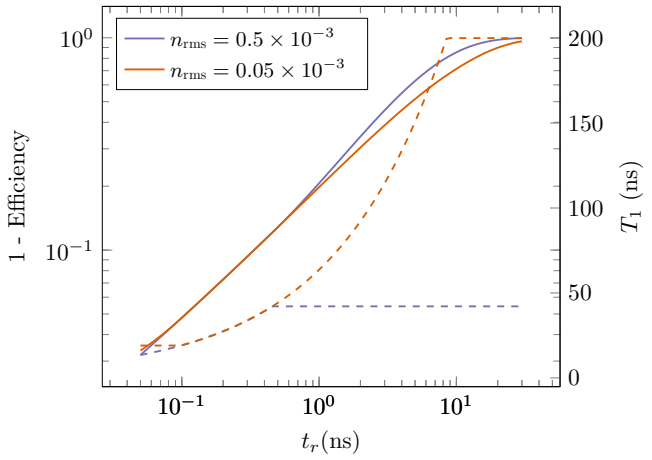

FIG. 4. Variation of usable emission probability (solid lines) and T_1 (dashed lines) for a CPB with rise time t_r for different levels of charge noise $n_{\rm rms}$. For $n_{\rm rms} = 0.5 \times 10^{-3}$, the linewidth is limited to 15 MHz, while for $n_{\rm rms} = 0.05 \times 10^{-3}$, the linewidth is limited to 5 MHz.

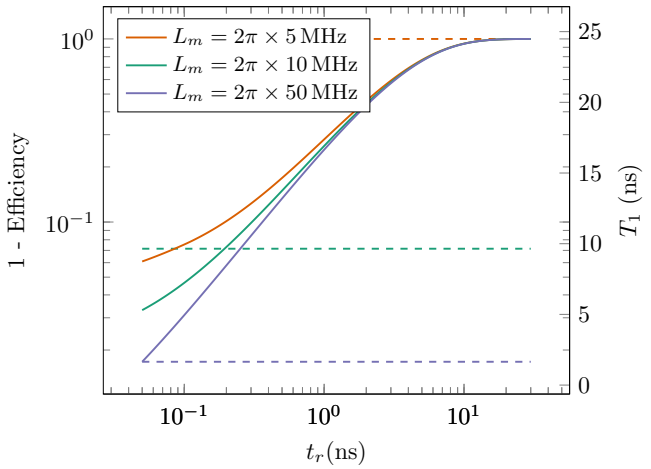

FIG. 5. Variation of usable emission probability (solid lines) and T_1 (dashed lines) for a flux qubit with rise time t_r for different maximum allowed linewidths L_m.

we neglect the contribution of charge noise for this system. For our analysis, we consider the values $\Delta/h \geq 1$ GHz and $\alpha = 0.7$, as these are shown to be achievable in fabrication [41,45]. Here, the usable efficiency monotonically increases with E_J (or equivalently I_c) for a fixed Δ [see Eqs. (12) and (15)]. We can therefore choose the maximum E_J that is allowed by our requirements on linewidth and repetition rate. For the flux qubit, the system-dependent decay [13,20,41] and decoherence rates [20] are approximated by

$$\Gamma_{1,o} = 2\frac{\omega Z (C_o \nu)^2}{\hbar}, \tag{20}$$

$$\Gamma_\phi = \sqrt{\varphi_{\rm rms}^2 \left(\frac{\partial \omega}{\partial \phi_e}\right)^2 + \frac{3\varphi_{\rm rms}^4}{4}\left(\frac{\partial^2 \omega}{\partial \phi_e^2}\right)^2}$$

$$\approx \frac{\varphi_{\rm rms} E_J \sqrt{1 - (1/2\alpha)^2}}{\hbar}, \tag{21}$$

$$\nu \approx \frac{E_J}{h} \times 10^{-7}\ \text{V/GHz}, \tag{22}$$

where the flux noise $\varphi_{\rm rms} \approx 10^{-5}\Phi_0$ [20].

To account for other sources of decay, we consider a contribution of $\Gamma_{\rm nr} = 2\ \mu\text{s}^{-1}$. As we would like to have the minimum possible Δ and maximum possible E_J, we limit the two values to $\Delta/h = 1$ GHz and $E_J/h \leq 250$ GHz. With these, we once again optimize the values of C_o and E_J to maximize usable efficiency while limiting the linewidth to a maximum allowed value. Finally, we also assume that, typically, a flux line can only sweep about $\pm 0.1\Phi_0$ around $0.5\Phi_0$ in a single step. With these considerations in mind, the optimized usable efficiencies and T_1 values are shown in Fig. 5 for three different maximum allowed linewidths $L_m/(2\pi)$ of 50, 10, and 5 MHz (note that for $E_J/h = 250$ GHz, the minimum linewidth is calculated to be about 2.5 MHz for our system).

Here, we once again see that for a rise time of 300 ps, we obtain efficiencies from about 87% to 92%, with the T_1 values being almost limited by the linewidths themselves, ranging from about 1.65 ns (repetition rate of 121 MHz) to about 25 ns (repetition rate of 8 MHz). The optimal capacitances also range from about 1.3 to 5.2 fF, which are achievable in fabrication.

Having claimed that the parameters needed to obtain around 90% usable efficiency are feasible for physical realization through fabrication, we now examine the robustness of these efficiencies to fabrication errors. In particular, we focus on fabrication errors in the parameters E_J and C_o, to which device performance is most sensitive. We allow for a 10% error in C_o and E_J for both the flux qubit and the CPB and plot the resulting range as error bars for the cases of $n_{\rm rms} = 0.5 \times 10^{-3}$ for the CPB, and a maximum allowed linewidth of 10 MHz for the flux qubit in Fig. 6. From the figure, we can see that at a rise time of around 300 ps, the uncertainty in the usable efficiency is only about 2% for both the CPB and the flux qubit. This suggests that, in addition to being able to provide reasonably high efficiencies, the system is reasonably robust to fabrication uncertainties.

Finally, using the obtained parameters, we can estimate the leakage of photons at the frequency of interest into the output line due to the parameter sweep. To account for this, we consider a trapezoidal pulse of amplitude 1 with rise time and fall time t_r, pulse width $T/2$, and period T. The envelope of the spectral function is given by ($\text{sinc}(x) =$

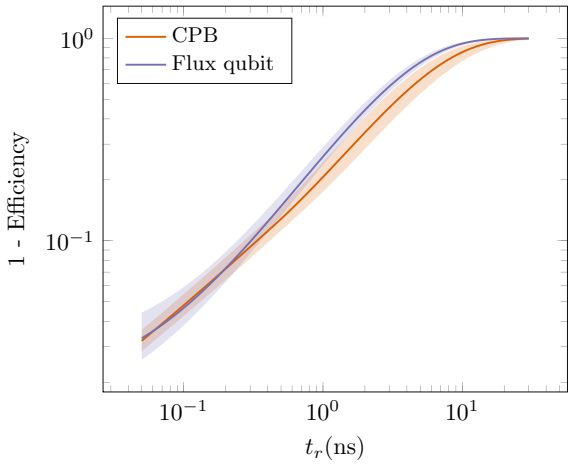

FIG. 6. Effect of fabrication uncertainty on the efficiency of the CPB (orange) and the flux qubit (blue). For both, the error range considers a 10% uncertainty in the Josephson energy E_J and the output capacitance C_o. The solid lines denote the "optimal" parameters for the given limits on linewidth and repetition rate, and the shaded regions of the same color indicate the uncertainty in the "inefficiency".

$\sin(\pi x)/(\pi x)$)

$$\left|S_{\text{trap}}(\omega)\right| \leq \frac{1}{2}\text{sinc}\left(\frac{\omega T}{4}\right)\text{sinc}\left(\frac{\omega t_r}{2}\right) \leq \frac{1}{2}\text{sinc}\left(\frac{\omega T}{4}\right). \tag{23}$$

Here, the average total power $\mathcal{P}$ is approximated by $(2e)^2/(C_g T)$ for a charge qubit and upper bounded by $(E_J + \Phi_0^2/2M)/T$ for a flux qubit. Using this, the power associated with the signal at $\omega \pm \Gamma$ can be approximated as $P_{l,\text{trap}} = (2\Gamma T)\mathcal{P}\left|S_{\text{trap}}(\omega)\right|^2$, where 2Γ is the frequency range of interest around ω (this can be taken to be the linewidth for a resonator or qubit).

Another estimate is obtained by considering a triangular pulse of amplitude 1 with rise time and fall time t_r. The envelope of the spectral function is given by

$$|S_{\text{tri}}(\omega)| = \text{sinc}^2\left(\frac{\omega t_r}{2}\right). \tag{24}$$

Once again, the power associated with the signal at $\omega \pm \Gamma$ can be approximated as $P_{l,\text{tri}} = (3\Gamma t_r/2)\mathcal{P}\,|S_{\text{tri}}(\omega)|^2$. Here, however, $\mathcal{P} \approx (2e)^2/(C_g t_r)$ for a charge qubit and $\approx (E_J + \Phi_0^2/2M)/t_r$ for a flux qubit.

Using this, one can estimate that the power leakage corresponds to a photon leakage of $\beta_c P_l/(\hbar\omega\Gamma)$, where Γ is the linewidth of our charge or flux qubit at the frequency of interest, and $\beta_c \in [0, 1]$ is a factor corresponding to the coupling between the sweeping line and the output line.

With the above recommended parameters for a CPB-based system, we obtain $P_l/(\hbar\omega\Gamma) \approx 0.07$ in the worst case of $\beta_c = 1$, assuming a triangular pulse. Hence, for $\beta \approx \left|2iZ\omega(C_o + C_g)\right|^2 \sim 10^{-5}$ in our system, we conclude that this does not limit the usability of the device. Similarly, for the flux-qubit-based architecture, we find that the leaked photon power $P_l/(\hbar\omega\Gamma) \approx 0.97$. Despite this comparatively large value of P_l for the flux qubit, the usability of the device is not limited by the photon leakage. This is because the flux line can be more effectively decoupled from the output line, even with $\beta_c \sim 10^{-3}$ (assuming that $\beta_c \approx |2Z\omega C_o|^2$).

Hence, we can see that both CPB and flux qubits are viable architectures for implementing a microwave-free single-photon generation protocol, with each having its own advantages. In a case in which there is limited control over the noise in the system, we recommend the use of a flux qubit. This is mainly because the linewidth of a flux qubit is not primarily due to T_ϕ but due to T_1 processes. Conversely, for a CPB, T_ϕ determines the linewidth, thus necessitating more complex noise-mitigation strategies during design and fabrication, as well as during measurements.

V. SUMMARY AND CONCLUSIONS

In summary, we propose a microwave-free excitation protocol for superconducting qubits using diabatic Landau-Zener transitions. Single microwave photons can then be generated via spontaneous emission from the excited state. Our theoretical estimates suggest that this protocol can be used for both Cooper-pair-box and flux-qubit-based architectures. Realizing robust quantum communication and cryptography systems requires high-efficiency, high-purity broadband generation of single photons. We have demonstrated that our method can be a key step in achieving this. We have theoretically demonstrated a high efficiency (>85%), high purity (leakage $<10^{-3}$) source with a very fast control of the emitted photon frequency over two octaves (from $\lesssim 3$ to $\gtrsim 12$ GHz). This fast control of photon frequencies, along with the high output rate and low footprint, makes this proposed architecture attractive for multiplexed setups where a single device can distribute its generation rate to supply photons to multiple channels separated in frequency. In addition to this, the proposed method has the advantage that it can be greatly improved upon with the development of better control-electronics hardware, allowing for the generation of pulses with shorter rise times and enabling even higher single-photon generation rates. While the current form of the protocol does not allow for pulse shaping of the emitted photons, we believe that can be achieved with further studies.

ACKNOWLEDGMENTS

The authors acknowledge the support of DST-INSPIRE Fellowship No. IF180339 and DST-SERB Core Research

Grant No. CRG/2018/002129. S.H. acknowledges the support of the Kishore Vaigyanik Protsahan Yojana (KVPY). S.H. also acknowledges helpful discussions with Harsh Arora and Johannes Fink.

APPENDIX A: A DERIVATION OF LZ TRANSITION PROBABILITY

In this appendix, we rederive the probability of transition for a Landau-Zener Hamiltonian, as described in Ref. [27], in modern notation. The eigenstates of the system at any given point of time are ψ_1 and ψ_2. These are also called the adiabatic basis of the system. The initial Hamiltonian in the adiabatic basis is defined as

$$H = \begin{pmatrix} \mathcal{E}_1 & 0 \\ 0 & \mathcal{E}_2 \end{pmatrix}. \tag{A1}$$

The evolution in this basis is difficult to manage because ψ_1 and ψ_2 evolve with $\mathcal{E}_1$ and $\mathcal{E}_2$.

To make the solution easier, we consider another basis ϕ_1 and ϕ_2, called the diabatic basis of the system, such that the Hamiltonian in this basis is given by

$$H = \begin{pmatrix} E_1 & E_{12} \\ E_{12} & E_2 \end{pmatrix}, \tag{A2}$$

and the system evolves such that

$$E_1 - E_2 = \hbar\alpha t, \quad E_1(0) = E_0, \quad \dot{E}_{12} = \dot{\phi_1} = \dot{\phi_2} = 0. \tag{A3}$$

One also observes that at $t \to -\infty$, $\phi_1 \to \psi_1$, and $\phi_2 \to \psi_2$, but as $t \to \infty$, $\phi_1 \to \psi_2$, and $\phi_2 \to \psi_1$.

In the most general form, we can see that the Hamiltonian can be written as

$$H(t) = \begin{pmatrix} E_0 & E_{12} \\ E_{12} & E_0 \end{pmatrix} + \begin{pmatrix} \hbar\alpha/2 & 0 \\ 0 & -\hbar\alpha/2 \end{pmatrix} t. \tag{A4}$$

Therefore, a general state can be written as $(c_1 \quad c_2)^T$. Writing the Schrodinger equation, we have

$$i\hbar \frac{\partial}{\partial t} \begin{pmatrix} c_1 \\ c_2 \end{pmatrix} = \begin{pmatrix} E_1 & E_{12} \\ E_{12} & E_2 \end{pmatrix} \begin{pmatrix} c_1 \\ c_2 \end{pmatrix} = \begin{pmatrix} E_1 c_1 + E_{12} c_2 \\ E_{12} c_1 + E_2 c_2 \end{pmatrix}. \tag{A5}$$

To convert this into a more manageable form, taking inspiration from evolution in nonperturbed systems, we write

$$\begin{pmatrix} c_1 \\ c_2 \end{pmatrix} = \begin{pmatrix} a e^{-i\int E_1 \, \mathrm{d}t/\hbar} \\ b e^{-i\int E_2 \, \mathrm{d}t/\hbar} \end{pmatrix}. \tag{A6}$$

Substituting this into Eq. (A5) and simplifying, we get

$$i\hbar \begin{pmatrix} \dot{a} \\ \dot{b} \end{pmatrix} = E_{12} \begin{pmatrix} b e^{i\int \alpha t \, \mathrm{d}t} \\ a e^{-i\int \alpha t \, \mathrm{d}t} \end{pmatrix}. \tag{A7}$$

Taking time derivatives on both sides and back-substituting into Eq. (A7), we obtain

$$0 = \ddot{a} - i\alpha t\dot{a} + \left(\frac{E_{12}}{\hbar}\right)^2 a, \tag{A8}$$

$$0 = \ddot{b} + i\alpha t\dot{b} + \left(\frac{E_{12}}{\hbar}\right)^2 b. \tag{A9}$$

As we are only interested in the values at $t \to \pm\infty$, where $\langle\phi_1|\phi_2\rangle = 0$, we need to solve for only one of these variables. We will choose to solve for b, with the boundary conditions being

$$|c_1(-\infty)| = |a(-\infty)| = 1, \tag{A10}$$

$$|c_2(-\infty)| = |b(-\infty)| = 0. \tag{A11}$$

To convert the differential equation into a more manageable form (with the aim of removing the $\dot{b}$ term), we substitute $b = v e^{-(i/2)\int \alpha t \, \mathrm{d}t}$ into Eq. (A10). This simplifies the equation to

$$\ddot{v} + \left(\left(\frac{E_{12}}{\hbar}\right)^2 - \frac{i\alpha}{2} + \frac{\alpha^2 t^2}{4}\right) v = 0. \tag{A12}$$

This is a *parabolic cylindrical equation*. To convert this into the standard form, we substitute

$$z = \sqrt{\alpha} e^{-i\pi/4} t, \quad \xi = \frac{1}{\alpha}\left(\frac{E_{12}}{\hbar}\right)^2 \tag{A13}$$

into the equation to get

$$\frac{\mathrm{d}^2 v}{\mathrm{d}z^2} - \left(-i\xi - \frac{1}{2} + \frac{z^2}{4}\right) v = 0. \tag{A14}$$

Observe that ξ can be used as a heuristic for the rate of the parameter sweep.

We know from Ref. [46] that equations of the form

$$\frac{\mathrm{d}^2 w}{\mathrm{d}z^2} - \left(a + \frac{z^2}{4}\right) = 0$$

have solutions as $U(a, \pm z), V(a, \pm z), U(-a, \pm iz)$, $V(-a, \pm iz)$. These are called *parabolic cylindrical functions*.

To select which of these we want, we need to apply the second boundary condition in Eq. (A10). As these are at $t \to -\infty$, from Eq. (A13), we find that $|z| \to \infty$, and thus

$$\arg z = \begin{cases} 3\pi/4, & \text{if } \alpha > 0, \\ -\pi/4, & \text{if } \alpha < 0. \end{cases}$$

In these limits, using the expansions as described in Ref. [46], we can see that $|V| \neq 0$. We thus only consider the functions $U(a,z)$ and its alternative forms.

From Ref. [46],

$$U(a,z) \sim e^{-z^2/4} z^{-a-1/2}, \text{ if } |\arg z| < 3\pi/4, \quad \text{(A15)}$$

$$U(-a, \pm iz) \sim e^{z^2/4} (\pm i)^{a-1/2} z^{a-1/2}, \text{ if } |\arg(\pm iz)| < 3\pi/4. \quad \text{(A16)}$$

As one can see, $U(a,z), U(-a,iz)$ has a singularity for $\arg z = 3\pi/4$, so we are forced to use $U(-a,-iz)$ as the solution for $\alpha > 0$. Similarly, the expansion of $U(-a,-iz)$ does not work for $\arg z = -\pi/4$, so we must use either $U(a,z)$ or $U(-a,iz)$. By symmetry considerations (essentially, not wanting to solve for the prefactor twice), we use the solutions

$$v(z) = NU(-a, \mp iz), \quad \text{if } \alpha > 0, \ \alpha < 0 \text{ respectively.} \quad \text{(A17)}$$

Now, to find the value of N, or rather $|N|$ (because we do not care about a universal phase), we make use of the first boundary condition in Eq. (A10) along with Eq. (A7). Thus,

$$\lim_{t\to-\infty} |\dot{b}| = \lim_{t\to-\infty} \left| \frac{aE_{12}}{i\hbar} \right| = \lim_{t\to-\infty} |a| \left| \frac{E_{12}}{\hbar} \right| = \left| \sqrt{\alpha\xi} \right|.$$

Further, using the definition of v (solving only for the $\alpha > 0$ case because the other case also has the same $|N|$),

$$\begin{aligned} |\dot{b}| &= \left| \dot{v} - \frac{i\alpha t}{2} v \right| = \left| \frac{dz}{dt}\frac{dv}{dz} - \frac{i\alpha t}{2} v \right|, \\ \left| \sqrt{\xi} \right| &= \lim_{t\to-\infty} |N| \left| (-i) U'(-a,-iz) + \frac{z}{2} U(-a,-iz) \right| \\ &= \lim_{|z|\to\infty, \arg z = 3\pi/4} |N| \left| (-i) U'(-a,-iz) \right. \\ &\quad \left. \times \frac{z}{2} U(-a,-iz) \right| \\ &= |N| \, e^{\pi\xi/4}, \end{aligned}$$

which implies

$$|N| = \left| \sqrt{\xi} \right| e^{-\pi\xi/4}. \quad \text{(A18)}$$

We now just need to find the value that $|b|$ takes as $t \to \infty$ which, from Eq. (A13), corresponds to $|z| \to \infty$:

$$\arg z = \begin{cases} -\pi/4, & \text{if } \alpha > 0, \\ 3\pi/4, & \text{if } \alpha < 0. \end{cases}$$

Again, we would only be solving for the $\alpha > 0$ case, as the other case leads to the same form of results. For this, we use (again from Ref. [46]), for $|\arg z| \in (\pi/4, 5\pi/4)$, we use

$$U(a,z) \sim \frac{e^{-z^2/4}}{z^{a+1/2}} \pm \frac{i\sqrt{2\pi}}{\Gamma(a+1/2)} e^{\mp i\pi a} e^{z^2/4} z^{a-1/2}. \quad \text{(A19)}$$

Thus, when using $\arg(-iz) = -3\pi/4$, we would need to use the minus sign above. Transforming, in the limit, we get

$$\lim_{|z|\to\infty, \arg z = -\pi/4} v = N \lim_{R\to\infty} \left(\frac{\sqrt{2\pi}}{\Gamma(i\xi+1)} e^{-\pi\xi/4} e^{iR^2/4} R^{i\xi} \right). \quad \text{(A20)}$$

Using $|\Gamma(1+ib)|^2 = \pi b/\sinh \pi b$, this implies

$$\lim_{|z|\to\infty, \arg z = -\pi/4} |v|^2 = 2e^{-\pi\xi} \sinh(\pi\xi). \quad \text{(A21)}$$

This is exactly the result in Ref. [27]. We can also rewrite this result in a more revealing form to see that

$$\lim_{t\to\infty} |c_2(t)|^2 = 1 - e^{-2\pi\xi}, \quad \text{(A22)}$$

or equivalently,

$$P_{g\to e} = e^{-2\pi\xi}. \quad \text{(A23)}$$

APPENDIX B: INTRODUCTION TO THE COOPER-PAIR BOX AND DESIGN FOR PHOTON EXTRACTION

The classical Hamiltonian for a Cooper-pair box (Fig. 7) is given by Refs. [34,35]

$$\begin{aligned} H &= \frac{(Q + C_g V_g)^2}{2(C_g + C_J)} - E_J \cos\left(\frac{2\pi\phi}{\Phi_0}\right) \\ &= E_Q \left(\frac{Q + C_g V_g}{2e} \right)^2 - E_J \cos\left(\frac{2\pi\phi}{\Phi_0}\right), \end{aligned} \quad \text{(B1)}$$

where $E_Q = (2e)^2/(2C_\Sigma)$, in which C_Σ is the capacitance of the island to its environment. Further defining $Q = 2ne$, $C_g V_g = -2n_g e$, and $\delta = 2\pi\phi/\Phi_0$, making use of the fact

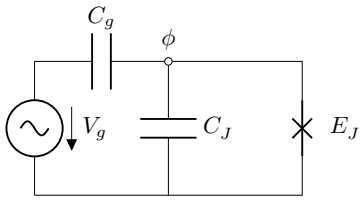

FIG. 7. Gate-biased Cooper-pair box.

that $[\hat{Q},\hat{\phi}] = -i\hbar \equiv [\hat{\delta},\hat{n}] = i$, we can show that up to constant terms, the quantum Hamiltonian is

$$\hat{H} = E_Q \sum_{n\in\mathbb{Z}} (n^2 - 2nn_g)\,|n\rangle\langle n| - \frac{E_J}{2}\sum_{n\in\mathbb{Z}} (|n\rangle\langle n+1| + |n+1\rangle\langle n|)\,. \tag{B2}$$

The design of the device in Fig. 7, has no way of extracting the photons generated by the system. To allow for extraction, we propose a device as shown in Fig. 8.

Introducing the transmission lines with the extra capacitances does not change the form of the Hamiltonian (excluding the transmission-line terms), but it has the effect of altering the value of C_Σ, which is now given by (details derived in Appendix C)

$$C_\Sigma = C_J + \frac{C_g}{1+\frac{k_m}{\beta_g}} + \frac{C_o}{1+\frac{k_m}{\beta_o}} = C_J + C_{g,\text{eff}} + C_{o,\text{eff}}, \tag{B3}$$

where k_m is the maximum wavenumber of the signal allowed by the transmission lines (which we hypothesize would be close to the superconducting gap equivalent of the film used, approximately 90 GHz for aluminum or approximately 1.1 THz for NbTiN). For frequencies greater than this, the dissipation becomes too great. Additionally, $\beta_{g/o} = c/C_{g/o}$, where c is the capacitance per unit length of the transmission line used. The frequency equivalent of β is about $3.2/C$ THz, where C is in fF for a 50Ω coplanar waveguide on silicon with $\epsilon_r \approx 11.7$.

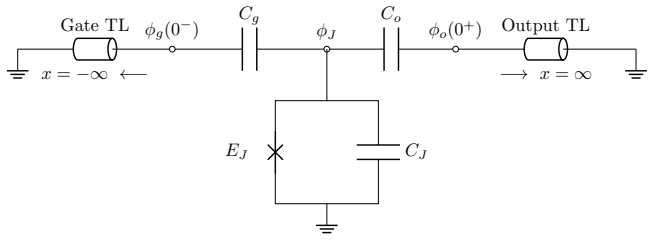

FIG. 8. Gate-biased Josephson junction with an output coupling and input and output lines. Here, C_g is the gate capacitance and C_o is the capacitance to the output line.

APPENDIX C: DERIVING THE EFFECT OF TRANSMISSION LINES ON THE CPB

We can write the Lagrangian corresponding to Fig. 8 as

$$\mathcal{L} = \mathcal{L}_o + \mathcal{L}_g + \mathcal{L}_Q + \mathcal{L}_{Cg} + \mathcal{L}_{Co}, \tag{C1}$$

where for l and c represent the inductance and capacitance per unit length of the transmission lines, respectively:

$$\mathcal{L}_o = \frac{1}{2}\int_{0^+}^{\infty} \mathrm{d}x \left(c\dot{\phi}_o^2(x,t) - \frac{1}{l}\phi_o'^2(x,t)\right), \tag{C2}$$

$$\mathcal{L}_g = \frac{1}{2}\int_{-\infty}^{0^-} \mathrm{d}x \left(c\dot{\phi}_g^2(x,t) - \frac{1}{l}\phi_g'^2(x,t)\right), \tag{C3}$$

$$\mathcal{L}_Q = \frac{1}{2}C_J\dot{\phi}_J^2 + E_J\cos\left(\frac{2\pi\phi_J}{\phi_0}\right), \tag{C4}$$

$$\mathcal{L}_{C_{g/o}} = \frac{1}{2}C_{g/o}(\dot{\phi}_J - \dot{\phi}_{g/o}(0,t))^2. \tag{C5}$$

Now, as we intend to excite the CPB using a voltage pulse on the charge line, we need to solve for the evolution of the input and output transmission lines along with the CPB. To do so, we would first write the transmission-line Lagrangian in k space by writing (hereafter, time dependence is implicitly assumed)

$$\phi_{g/o}(x) = \int_0^\infty \mathrm{d}k(q_{g/o}(k)\cos(kx) + p_{g/o}(k)\sin(kx)), \tag{C6}$$

where $Z = \sqrt{l/c}$ is the characteristic impedance of the transmission lines, and q and p are Fourier coefficients corresponding to a real ϕ. Hence, using the orthogonality of $\cos(kx)$ and $\sin(kx)$, we can rewrite the Lagrangian as (for $\omega_k = vk$ and $v = 1/\sqrt{lc}$, the speed of light in the transmission line)

$$\mathcal{L}_{g/o} = \frac{1}{2}\int_0^\infty \mathrm{d}k \left(c(\dot{q}_{g/o}^2 + \dot{p}_{g/o}^2) - \frac{k^2}{l}(q_{g/o}^2 + p_{g/o}^2)\right), \tag{C7}$$

$$\mathcal{L}_{C_{g/o}} = \frac{1}{2}C_{g/o}\left(\dot{\phi}_J^2 - 2\dot{\phi}_J\int_0^\infty \mathrm{d}k\dot{q}_{g/o}(k) + \left(\int_0^\infty \mathrm{d}k\dot{q}_{g/o}(k)\right)^2\right). \tag{C8}$$

The primary observation of interest here is that only the $q_{g/o}$ terms couple with the CPB. We can now write the

momenta as

$$\frac{\partial \mathcal{L}}{\partial \dot{\phi}_J} = Q_J = C_J\dot{\phi}_J + C_o\left(\dot{\phi}_J - \int_0^\infty \mathrm{d}k'\dot{q}_o(k')\right) + C_g\left(\dot{\phi}_J - \int_0^\infty \mathrm{d}k'\dot{q}_g(k')\right), \tag{C9}$$

$$\frac{\partial \mathcal{L}}{\partial \dot{q}_{g/o}(k)} = r_{g/o}(k) = c\dot{q}_{g/o}(k) - C_{g/o}\left(\dot{\phi}_J - \int_0^\infty \mathrm{d}k'\dot{q}_{g/o}(k')\right), \tag{C10}$$

$$\frac{\partial \mathcal{L}}{\partial \dot{p}_{g/o}(k)} = s_{g/o}(k) = \frac{\dot{p}_{g/o}(k)}{\omega_k}. \tag{C11}$$

If one tries to solve this directly, one gets tangled up in an intractable web of infinities and zeroes. To alleviate us from this burden, we assume that the transmission line can only support modes up to a cutoff k_m, i.e., $q_{g/o}(k > k_m) = p_{g/o}(k > k_m) = 0$. Back-substituting for $\dot{q}_g$ in the integral and letting $\beta_J = c/C_J$, $\beta_g = c/C_g$, and $\beta_o = c/C_o$, we get

$$\int_0^{k_m} \mathrm{d}k'\dot{q}_g(k') = \frac{1}{c\left(1+\frac{k_m}{\beta_g}\right)}\int_0^{k_m}\mathrm{d}k' r_g(k') + \frac{k_m/\beta_g}{1+\frac{k_m}{\beta_g}}\dot{\phi}_J, \tag{C12}$$

$$\int_0^{k_m} \mathrm{d}k'\dot{q}_o(k') = \frac{1}{c\left(1+\frac{k_m}{\beta_o}\right)}\int_0^{k_m}\mathrm{d}k' r_o(k') + \frac{k_m/\beta_o}{1+\frac{k_m}{\beta_o}}\dot{\phi}_J. \tag{C13}$$

Substituting this into the expressions for momenta, defining $I_g = \int_0^{k_m}\mathrm{d}k r_g(k)$ and $I_o = \int_0^{k_m}\mathrm{d}k r_o(k)$, writing the Hamiltonian as

$$\mathcal{H} = \int_0^{k_m} r_g(k)\dot{q}_g(k)\,\mathrm{d}k + \int_0^{k_m} r_o(k)\dot{q}_o(k)\,\mathrm{d}k + \int_0^{k_m} s_g(k)\dot{p}_g(k)\,\mathrm{d}k + \int_0^{k_m} s_o(k)\dot{p}_o(k)\,\mathrm{d}k + Q_J\dot{\phi}_J - \mathcal{L},$$

and substituting and simplifying, we get

$$\mathcal{H} = \frac{\left(Q_J - \left(\frac{I_g}{k_m+\beta_g} + \frac{I_o}{k_m+\beta_o}\right)\right)^2}{2c\left(\frac{1}{\beta_J} + \frac{1}{k_m+\beta_g} + \frac{1}{k_m+\beta_o}\right)} - E_J\cos\left(\frac{2\pi\phi_J}{\phi_0}\right) - \frac{I_g^2}{2c(\beta_g+k_m)} - \frac{I_o^2}{2c(\beta_o+k_m)} + \frac{1}{2}\int_0^{k_m}\mathrm{d}k\left(\frac{r_g^2(k)+s_g^2(k)}{c} + k^2\frac{q_g^2(k)+p_g^2(k)}{l}\right) + \frac{1}{2}\int_0^{k_m}\mathrm{d}k\left(\frac{r_o^2(k)+s_o^2(k)}{c} + k^2\frac{q_o^2(k)+p_o^2(k)}{l}\right). \tag{C14}$$

This expression suggests that this system still acts as a charge qubit, although the coupling contributions are scaled down based on the modes allowed by the transmission line.

We can rewrite this in terms of standard quantities for a charge qubit as

$$\mathcal{H} = E_Q\left(N_J - N_g - N_o\right)^2 - E_J\cos(\delta) - \frac{(2e)^2N_g^2(\beta_g+k_m)}{2c} - \frac{(2e)^2N_o^2(\beta_o+k_m)}{2c} + \frac{1}{2}\int_0^{k_m}\mathrm{d}k\left(\frac{r_g^2(k)+s_g^2(k)}{c} + k^2\frac{q_g^2(k)+p_g^2(k)}{l}\right) + \frac{1}{2}\int_0^{k_m}\mathrm{d}k\left(\frac{r_o^2(k)+s_o^2(k)}{c} + k^2\frac{q_o^2(k)+p_o^2(k)}{l}\right). \tag{C15}$$

where

$$E_Q = \frac{(2e)^2}{2\left(C_J + \frac{C_g}{1+k_m/\beta_g} + \frac{C_o}{1+k_m/\beta_o}\right)}, \tag{C16}$$

$$N_{g/o} = \frac{I_{g/o}}{k_m+\beta_{g/o}}, \tag{C17}$$

$$\delta = \frac{2\pi\phi_J}{\phi_0}. \tag{C18}$$

Looking at the corresponding contributions to the charging energy, we also define

$$C_{g/o,\mathrm{eff}} = \frac{C_{g/o}}{1+k_m/\beta_{g/o}}. \tag{C19}$$

APPENDIX D: EFFECT OF PULSE SHAPE ON THE PROBABILITY OF DIABATIC EXCITATIONS

To study the effect of the pulse shape for sweeps that are not linear (fixed rate), we resort to numerical simulations, as analytical expressions are difficult to obtain. For the simulations, we consider a CPB and a few common nonlinear pulse shapes (shown in the inset of Fig. 9)—namely half-Gaussian ($\sigma = t_r/3$), tanh ($k = t_r/3$), and exponential—and compare them to a linear ramp-shaped pulse. All

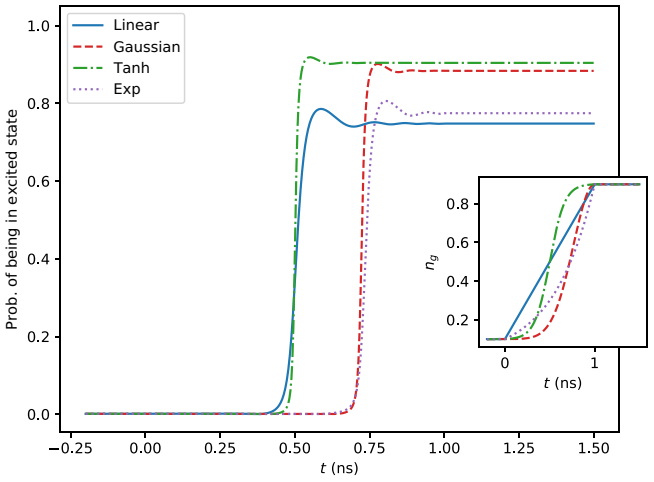

FIG. 9. Simulated evolution of the probability of the CPB to be in the first excited state for a rise time of 1 ns from $n_g = 0.1$ to $n_g = 0.9$. The inset shows the pulse shapes corresponding to the rise.

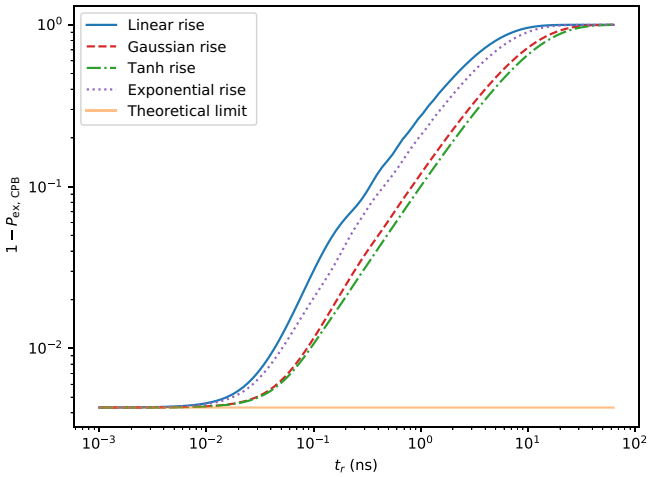

FIG. 10. Simulated probability that the CPB is not in an excited state as a function of rise time for different pulse shapes.

the simulations presented use $E_J/h = 1$ GHz and $E_Q/h = 19.27$ GHz for the CPB, considering levels from $n = -3$ through $n = 4$ to solve the Schrödinger equation [47,48]. We note that any further increase in the number of levels does not change the simulations up to a relative error of 10^{-9}. The pulses start at $t = 0$ with $n_g = n_i$ and end at $t = t_r$ with $n_g = n_f$. For a rise time of t_r, the pulse shapes for $0 \le t \le t_r$ are given by the expressions ($\tau = t/t_r$)

$$\text{Linear rise: } \frac{n_g(\tau) - n_i}{n_f - n_i} = \tau, \tag{D1}$$

$$\text{Gaussian rise: } \frac{n_g(\tau) - n_i}{n_f - n_i} = \frac{e^{-9(1-\tau)^2} - e^{-9}}{1 - e^{-9}}, \tag{D2}$$

$$\text{Tanh rise: } \frac{n_g(\tau) - n_i}{n_f - n_i} = \frac{1 + \dfrac{\tanh((\tau - 0.5) \times 6)}{\tanh(3)}}{2}, \tag{D3}$$

$$\text{Exponential rise: } \frac{n_g(\tau) - n_i}{n_f - n_i} = \frac{(n_f/n_i)^\tau - 1}{n_f/n_i - 1}. \tag{D4}$$

The evolution of the probability of the system remaining unexcited for different total rise times is shown in Fig. 9. From this figure, we observe that the "excitation" of the system happens primarily when the swept parameter $\chi \equiv n_g$ traverses the avoided crossing. This justifies the inclusion of the additional step of going from χ_i to $-\chi_0/2$ to optimize the excitation, as the probability of excitation of the system is negligible during this step.

From the plot of excitation probabilities vs rise times shown in Fig. 10, we can observe that for a given rise time, a greater probability of excitation is achieved for the pulse shapes where the rate of sweeping is higher near the avoided crossing. This behavior is in agreement with our expectations. The probabilities can be well approximated by linearizing the pulses around the avoided crossing. This is clearly illustrated in the plot of excitation probabilities vs effective rise time ($t_{r,\text{eff}} = (n_f - n_i)/\dot{n}_g(n_g^{-1}(0.5))$) shown in Fig. 11. Hence, we claim that a linear sweep is sufficient for all hardware configurations. Another important fact that we observe from Fig. 10 is that at the lowest sweep times, the probability of not being in the excited state saturates to a value of approximately 0.4%. This saturation can be explained by the fact that the ground state of the system at the beginning of the pulse is not exactly the same as the excited state of the system at the end of the pulse for a multilevel Hamiltonian. To account for this, the "theoretical limit" line has been plotted to signify the value of $|\langle g, t = 0 | e, t = t_r \rangle|^2$, which is the maximum success

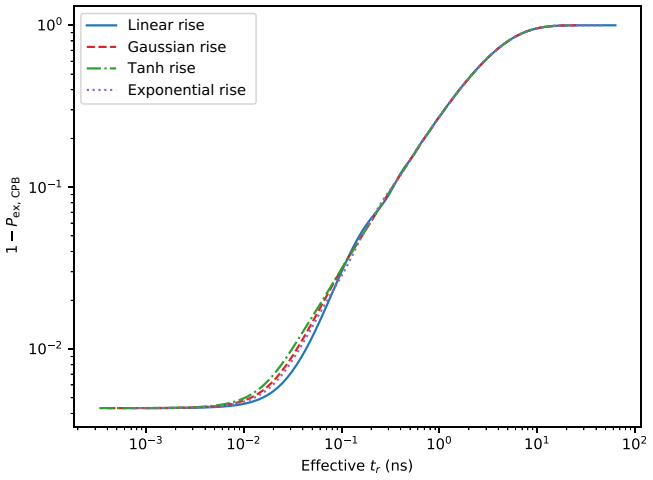

FIG. 11. Simulated probability that the CPB is not in the first excited state as a function of effective rise time for different pulse shapes.

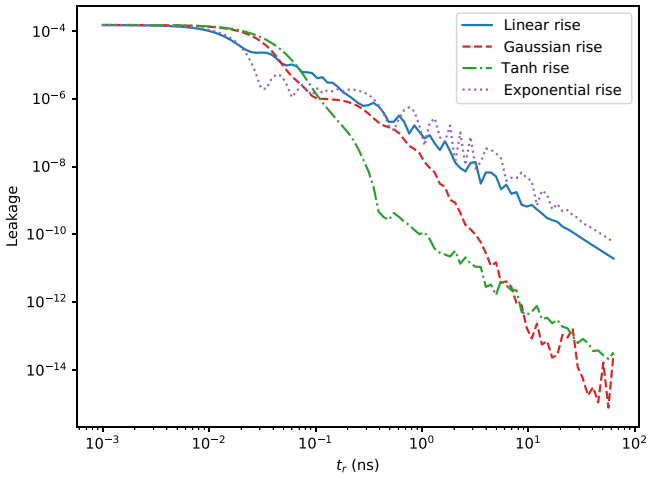

FIG. 12. Effect of rise time (t_r) on the leakage.

probability allowed for a perfect (infinitely fast) diabatic transition.

APPENDIX E: LEAKAGE OF EXCITATIONS TO OUTSIDE THE $|g\rangle, |e\rangle$ SUBSPACE

To study the effect of the pulse sequence on leakage to outside the $|g\rangle, |e\rangle$ subspace of interest, we solve the Schrödinger equation for a CPB with $E_J/h = 1$ GHz and $E_Q/h = 19.27$ GHz, considering the levels $n = -3$ through $n = 4$. First, we look at the effect of rise time on leakage for pulses that start from $n_{g,\min} = 0.1$ and go to $n_{g,\max} = 0.9$ (the avoided crossing occurs at $n_g = 0.5$). The results are shown in Fig. 12.

From the figure, we observe that for low enough rise times, the leakage saturates to a low value of about 1.5×10^{-4}. We also note that the leakage to outside the subspace contributing to multiphoton events in the output is much lower for the case of the Gaussian and tanh pulses than for the linear and exponential rises. Still, we would like to point out that for currently accessible rise times of $\gtrsim 100$ ps, the leakage to higher states due to a linear pulse is $\lesssim 10^{-6}$.

Having studied the effect of the rise time of the pulse, we conducted further simulations to check the effect of the range of the sweep. We fixed a rise time of 1 ns and simulated the effect of pulses where n_g is swept linearly from $n_{g,\min}$ to $1 - n_{g,\min}$. The results of these simulations can be seen in Fig. 13. Based on these simulations, we claim that it is sufficient to employ a linear pulse for reasonably high-purity single-photon generation at the output.

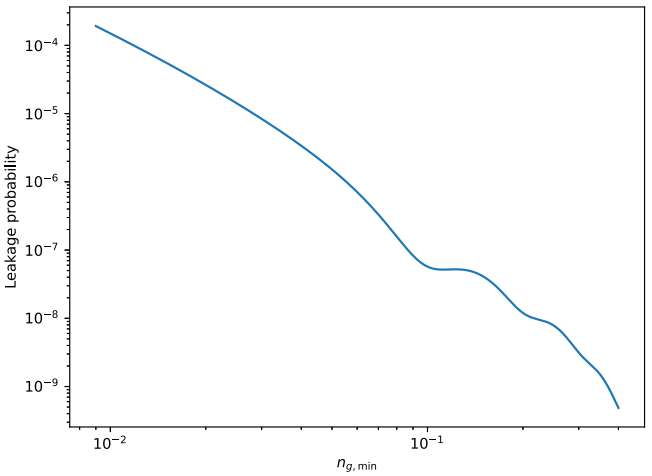

FIG. 13. Effect of the range of sweep on the leakage.

[1] M. D. Eisaman, J. Fan, A. Migdall, and S. V. Polyakov, Invited Review Article: Single-photon sources and detectors, Rev. Sci. Instrum. **82**, 071101 (2011).

[2] M. Pechal, L. Huthmacher, C. Eichler, S. Zeytinoğlu, A. A. Abdumalikov, S. Berger, A. Wallraff, and S. Filipp, Microwave-controlled generation of shaped single photons in circuit quantum electrodynamics, Phys. Rev. X **4**, 041010 (2014).

[3] P. Forn-Díaz, C. W. Warren, C. W. S. Chang, A. M. Vadiraj, and C. M. Wilson, On-demand microwave generator of shaped single photons, Phys. Rev. Appl. **8**, 054015 (2017).

[4] E. Knill, R. Laflamme, and G. J. Milburn, A scheme for efficient quantum computation with linear optics, Nature **409**, 46 (2001).

[5] Han-Sen Zhong *et al.*, Quantum computational advantage using photons, Science **370**, 1460 (2020).

[6] Pieter Kok, W. J. Munro, Kae Nemoto, T. C. Ralph, Jonathan P. Dowling, and G. J. Milburn, Linear optical quantum computing with photonic qubits, Rev. Mod. Phys. **79**, 135 (2007).

[7] H. J. Kimble, The quantum internet, Nature **453**, 1023 (2008).

[8] H. Inamori, N. Lütkenhaus, and D. Mayers, Unconditional security of practical quantum key distribution, Eur. Phys. J. D **41**, 599 (2007).

[9] Charles H. Bennett and Gilles Brassard, Quantum cryptography: Public key distribution and coin tossing, Theor. Comput. Sci. **560**, 7 (2014).

[10] Artur K. Ekert, Quantum cryptography based on Bell's theorem, Phys. Rev. Lett. **67**, 661 (1991).

[11] L.-M. Duan, M. D. Lukin, J. I. Cirac, and P. Zoller, Long-distance quantum communication with atomic ensembles and linear optics, Nature **414**, 413 (2001).

[12] C. L. Degen, F. Reinhard, and P. Cappellaro, Quantum sensing, Rev. Mod. Phys. **89**, 035002 (2017).

[13] Z. H. Peng, S. E. de Graaf, J. S. Tsai, and O. V. Astafiev, Tuneable on-demand single-photon source in the microwave range, Nat. Commun. **7**, 12588 (2016).

[14] Ming Li, Juan José García-Ripoll, and Tomás Ramos, Scalable multiphoton generation from cavity-synchronized single-photon sources, Phys. Rev. Res. **6**, 033295 (2024).

[15] Christian Kurtsiefer, Sonja Mayer, Patrick Zarda, and Harald Weinfurter, Stable solid-state source of single photons, Phys. Rev. Lett. **85**, 290 (2000).

[16] Christian Brunel, Brahim Lounis, Philippe Tamarat, and Michel Orrit, Triggered source of single photons based on controlled single molecule fluorescence, Phys. Rev. Lett. **83**, 2722 (1999).

[17] J. Hours, S. Varoutsis, M. Gallart, J. Bloch, I. Robert-Philip, A. Cavanna, I. Abram, F. Laruelle, and J. M. Gérard, Single photon emission from individual GaAs quantum dots, Appl. Phys. Lett. **82**, 2206 (2003).

[18] Yu-Jia Wei, Yu-Ming He, Ming-Cheng Chen, Yi-Nan Hu, Yu He, Dian Wu, Christian Schneider, Martin Kamp, Sven Höfling, Chao-Yang Lu, and Jian-Wei Pan, Deterministic and robust generation of single photons from a single quantum dot with 99.5% indistinguishability using adiabatic rapid passage, Nano Lett. **14**, 6515 (2014).

[19] A. A. Houck, D. I. Schuster, J. M. Gambetta, J. A. Schreier, B. R. Johnson, J. M. Chow, L. Frunzio, J. Majer, M. H. Devoret, S. M. Girvin, and R. J. Schoelkopf, Generating single microwave photons in a circuit, Nature **449**, 328 (2007).

[20] Jens Koch, Terri M. Yu, Jay Gambetta, A. A. Houck, D. I. Schuster, J. Majer, Alexandre Blais, M. H. Devoret, S. M. Girvin, and R. J. Schoelkopf, Charge-insensitive qubit design derived from the Cooper pair box, Phys. Rev. A **76**, 042319 (2007).

[21] Yu Zhou, Zhihui Peng, Yuta Horiuchi, O. V. Astafiev, and J. S. Tsai, Tunable microwave single-photon source based on transmon qubit with high efficiency, Phys. Rev. Appl. **13**, 034007 (2020).

[22] Yong Lu, Andreas Bengtsson, Jonathan J. Burnett, Baladitya Suri, Sankar Raman Sathyamoorthy, Hampus Renberg Nilsson, Marco Scigliuzzo, Jonas Bylander, Göran Johansson, and Per Delsing, Quantum efficiency, purity and stability of a tunable, narrowband microwave single-photon source, npj Quantum Inf. **7**, 1 (2021).

[23] Giuseppe Mangano, Jens Siewert, and Giuseppe Falci, Single photon generation in superconducting microwave cavities, Verh. Dtsch. Phys. Ges. **43**, 1 (2008).

[24] Shavindra P. Premaratne, F. C. Wellstood, and B. S. Palmer, Microwave photon Fock state generation by stimulated Raman adiabatic passage, Nat. Commun. **8**, 14148 (2017).

[25] Run-Ying Yan and Zhi-Bo Feng, Fast generation of microwave photon Fock states in a superconducting nanocircuit, Physica E **127**, 114522 (2021).

[26] Lev Davidovich Landau, Zur theorie der energieubertragung. II, Z. Sowjetunion **2**, 46 (1932).

[27] Clarence Zener and Ralph Howard Fowler, Non-adiabatic crossing of energy levels, Proc. R. Soc. London, Ser. A **137**, 696 (1932).

[28] E. C. G. Stueckelberg, Theorie der unelastischen Stösse zwischen Atomen, (1932).

[29] E. Majorana, Atomi orientati in campo magnetico variabile, Nuovo Cim. **9**, 43 (1932).

[30] A. V. Shytov, Landau–Zener transition in a multilevel system. An exact result, Phys. Rev. A **70**, 052708 (2004).

[31] Yu. N. Demkov and V. I. Osherov, Stationary and nonstationary problems in quantum mechanics that can be solved by means of contour integration, Sov. J. Exp. Theor. Phys. **26**, 916 (1968).

[32] Yu N. Demkov and V. N. Ostrovsky, The exact solution of the multistate Landau–Zener type model: The generalized bow-tie model, J. Phys. B: At. Mol. Phys. **34**, 2419 (2001).

[33] Nikolai A. Sinitsyn and Fuxiang Li, Solvable multistate model of Landau–Zener transitions in cavity QED, Phys. Rev. A **93**, 063859 (2016).

[34] Alexander Shnirman, Gerd Schön, and Ziv Hermon, Quantum manipulations of small Josephson junctions, Phys. Rev. Lett. **79**, 2371 (1997).

[35] Yuriy Makhlin, Gerd Schön, and Alexander Shnirman, Quantum-state engineering with Josephson-junction devices, Rev. Mod. Phys. **73**, 357 (2001).

[36] K. Bladh, T. Duty, D. Gunnarsson, and P. Delsing, The single Cooper-pair box as a charge qubit, New J. Phys. **7**, 180 (2005).

[37] This is allowed because the form of the n-independent terms is $n_g^2 \sum_n |n\rangle\langle n| = n_g^2 \cdot \mathbb{1}$. This term can be thought of as just a global reference potential offset that does not affect either the eigenstates or the transition frequencies of the Hamiltonian being studied.

[38] This is equivalent to choosing any other range of $n_g \in m + \epsilon_g, m + 1 - \epsilon_g$ for $m \in \mathbb{Z}$ for which the subspace of interest would be $n = m, m + 1$.

[39] J. E. Mooij, T. P. Orlando, L. Levitov, Lin Tian, Caspar H. van der Wal, and Seth Lloyd, Josephson persistent-current qubit, Science **285**, 1036 (1999).

[40] T. L. Robertson, B. L. T. Plourde, P. A. Reichardt, T. Hime, C.-E. Wu, and John Clarke, Quantum theory of three-junction flux qubit with non-negligible loop inductance: Towards scalability, Phys. Rev. B **73**, 174526 (2006).

[41] Frank Deppe, Superconducting Flux Quantum Circuits: Characterization, Quantum Coherence, and Controlled Symmetry Breaking, Ph.D. thesis, Technical University of Munich, Munich, Germany, 2009.

[42] Simon Burkhard, Optimization of Transmon Design for Longer Coherence Time, Master's thesis, ETH Zurich, 2012.

[43] A. B. Zorin, F.-J. Ahlers, J. Niemeyer, T. Weimann, H. Wolf, V. A. Krupenin, and S. V. Lotkhov, Background charge noise in metallic single-electron tunneling devices, Phys. Rev. B **53**, 13682 (1996).

[44] S. M. Verbrugh, M. L. Benhamadi, E. H. Visscher, and J. E. Mooij, Optimization of island size in single electron tunneling devices: Experiment and theory, J. Appl. Phys. **78**, 2830 (1995).

[45] Fei Yan, Simon Gustavsson, Archana Kamal, Jeffrey Birenbaum, Adam P. Sears, David Hover, Ted J. Gudmundsen, Danna Rosenberg, Gabriel Samach, S. Weber, Jonilyn L. Yoder, Terry P. Orlando, John Clarke, Andrew J. Kerman, and William D. Oliver, The flux qubit revisited to enhance coherence and reproducibility, Nat. Commun. **7**, 12964 (2016).

[46] Nico M. Temme, *Asymptotic Methods for Integrals*, Series in Analysis, Vol. 6 (World Scientific, New Jersey, 2015).

[47] J. R. Johansson, P. D. Nation, and Franco Nori, QuTiP: An open-source Python framework for the dynamics of open quantum systems, Comput. Phys. Commun. **183**, 1760 (2012).

[48] J. R. Johansson, P. D. Nation, and Franco Nori, QuTiP 2: A Python framework for the dynamics of open quantum systems, Comput. Phys. Commun. **184**, 1234 (2013).